Volume 1 | Number 1 | Jan 2013 | Pages 1–100

Nanoscale

www.rsc.org/nanoscale

ROYAL SOCIETY OF CHEMISTRY

ROYAL SOCIETY OF CHEMISTRY

www.rsc.org/nanoscale

Positively-charged Reduced Graphene Oxide as an Adhesion Promoter for Highly-stable Silver Nanowire Film

Qijun Sun [a,†], Seong Jun Lee [a,†], Hyungseok Kang[a], Yuseong Gim[a], Ho Seok Park[b], Jeong Ho Cho[a,b]*

Abstract Ultrathin conductive adhesion promoter using positively charged reduced graphene oxide (rGO-NH_3^+) are demonstrated for preparing highly stable silver nanowire transparent conductive electrodes (AgNW TCEs). The adhesion promoter rGO-NH_3^+ spray coated between the substrate and AgNWs significantly enhances both the chemical and mechanical stabilities of the AgNW TCEs. Besides, the ultrathin thickness of the rGO-NH_3^+ ensures the TCEs with excellent optical transparency and mechanical flexibility. The AgNW films prepared from the adhesion promoter are extremely stable under harsh conditions, including ultrasonication in a variety of solvents, 3M scotch tape detachment test, mechanical bending up to a 0.3% strain, fatigue over 1000 cycles. The greatly enhanced adhesion force is attributed to the ionic interactions between the positively charged protonated amine groups in rGO-NH_3^+ and the negatively charged hydroxo- and oxo-groups on the AgNWs. The positively charged GO-NH_3^+ and commercial polycationic polymer (poly allylamine hydrochloride) are also prepared as adhesion promoters for comparison with rGO-NH_3^+. Notably, the closely packed hexagonal atomic structure of rGO offers better barrier properties to water permeation and demonstrates promising utility in durable waterproof electronics. This work offers a simple method to prepare high-quality TCEs and is believed to have great potential application in flexible waterproof electronics.

---

[a] *SKKU Advanced Institute of Nanotechnology (SAINT), Sungkyunkwan University, Suwon 440-746, Republic of Korea.*

E-mail: jhcho94@skku.edu

[b] *School of Chemical Engineering, Sungkyunkwan University, Suwon 440-746, Republic of Korea.*

[†] *Q. Sun and S. J. Lee contributed equally to this work.*

Introduction

The increasing interest in flexible optoelectronic devices, such as touch screens, photovoltaic cells, liquid crystal displays (LCDs), and light emitting diodes (LEDs) has inspired concerted efforts toward the development of flexible transparent conductive electrodes (TCEs)[1-3]. The most TCEs commonly used in the industry are indium tin oxide (ITO)[4], which has a low sheet resistance (10–50 $\Omega \cdot sq^{-1}$) and a high optical transparency (90% across the visible range). ITO has several drawbacks, however, in that it is highly brittle, the cost of indium has increased as pressures on the limited mineral deposits have intensified[5], and ITO must be processed at high temperatures that are incompatible with flexible or bendable electronic substrates. Several alternative substrates have emerged, including conducting polymers[6], carbon nanomaterials[7, 8] (i.e. carbon nanotubes (CNTs) and graphene), and metallic grids[9, 10]. Unfortunately, the sheet resistances (on the order of several hundred $\Omega \cdot sq^{-1}$) and the optical profiles (80% transmittance) of the conducting polymers and of the carbon nanomaterials are inferior to those of ITO[8]. Metallic grid electrodes typically require complex fabrication procedures involving vacuum deposition of the metal films, photolithography, nanoimprint lithography (NIL), or transfer printing[9, 10].

Silver nanowires (AgNWs) dispersed in solvent have been explored as an alternative to ITO because they offer a low resistance, good optical transparency, and high mechanical flexibility[11-16]. A variety of low-cost fabrication processes for preparing flexible AgNW TCEs have been developed, including spin-coating[15, 16], air-spraying[14], and bar coating[12]. Previous AgNW studies have focused mainly on decreasing the sheet resistance using post-welding processes involving thermal, mechanical, and electrochemical treatments, or integration with other materials[17-20]. Another issue with the AgNWs is that the surface roughness must be reduced using a variety of overcoating layers applied onto the AgNW films, such as poly (3,4-ethylenedioxythiophene):poly (styrenesulfonate) (PEDOT:PSS)[21], zinc oxide[22, 23] or graphene oxide[24-26]. The high surface roughness of the AgNWs may create electrical shorts across the semiconducting layers because rigid nanowires can pile up and/or protrude to form locally high spikes. The adhesion between the AgNWs and the plastic substrate is especially critical to the durability of the TCEs. Despite its importance, few studies have attempted to address the adhesion issue. One approach involved depositing a polycationic polymer of poly(diallyldimethylammonium chloride) (PDDA) onto a AgNW film to enhance the interfacial adhesion between the AgNWs and the polymeric substrate[27]. Polycations, however, are typically soluble in water, which could prohibit their use as an adhesive in waterproof electronic devices based on AgNWs TCEs. Recently, silane-type self-assembled monolayers with a variety of end functional groups that engaged in coordination bonding with the Ag centers were used to improve adhesion and produce highly stretchable AgNWs electrodes[28]. However, long reaction times between the silane molecules and the hydroxyl-functionalized rubber surface were required to produce homogeneous surface grafting. Moreover, the non-conductive characters of both materials prohibited the preparation of a uniform current distribution

throughout the mesh-type AgNWs. The development of new conductive adhesion promoters with simplified fabrication processes is urgently required for the preparation of highly stable AgNW TCEs.

In this communication, we firstly demonstrated the preparation of ultrathin conductive adhesion promoters using positively charged reduced graphene oxide ($rGO-NH_3^+$) to fabricate highly stable transparent AgNW TCEs. The $rGO-NH_3^+$ layer was deposited using a simple spray-coating method onto the polymeric substrate. The ultrathin thickness of the $rGO-NH_3^+$ ensured excellent optical transparency and mechanical flexibility. The insertion of the $rGO-NH_3^+$ between the AgNWs and the polymeric substrate dramatically enhanced both the chemical and mechanical stabilities of the AgNW film. For example, the AgNW TCEs prepared with the adhesion promoter were extremely stable under harsh conditions, including ultrasonication in a variety of solvents, 3M scotch tape detachment test, mechanical bending up to a 0.3% strain, or fatigue over 1000 cycles. The strongly enhanced adhesion originated from the ionic interactions between the negatively charged hydroxo- and oxo-groups on the AgNWs[29] and the positively charged protonated amine groups in $rGO-NH_3^+$. For comparison, the positively charged $GO-NH_3^+$ or commercial poly(allylamine hydrochloride) (PAH) were applied as adhesion promoters. Notably, the closely packed hexagonal atomic structure of rGO also created a barrier to water permeation so that the ultrathin $rGO-NH_3^+$ adhesion promoter demonstrated promising utility in durable waterproof electronics.

Experiments

Sample preparation: Graphite oxide used in this work was synthesized through the modified Hummers method. A stable positively charged graphene oxide ($GO-NH_3^+$) suspension was prepared by introducing amine groups ($-NH_2$) onto the surfaces of the negatively charged GO sheets using N-ethyl-N'-(3-dimethyl aminopropyl) carbodiimide methiodide (EDC, 98%, Alfa Aesar) and ethylenediamine (99%, Sigma-Aldrich). $GO-NH_3^+$ suspensions were reduced using a hydrazine solution (35 wt% in water, Aldrich).

AgNWs TCE preparation: The polyethylene naphthalate (PEN) substrate was first treated with ultraviolet illumination under an ozone atmosphere. The $GO-NH_3^+$ and $rGO-NH_3^+$ suspensions were then spray-coated onto the hydroxyl-terminated PEN substrate. The surface coverage levels of both samples could be controlled by varying the spray-coating time. For comparison, commercially available poly(allylamine hydrochloride) (PAH) in distilled water (2 wt%) was spin-coated onto the PEN substrate. A 0.5 wt% AgNW solution suspended in isopropyl alcohol (purchased from Aldrich Chemical Co. with diameter = 115 nm and length = 20–50 mm) was coated onto the substrate using the Meyer rod coating method (#14, RD Specialist Inc.). Three post-processing welding steps, including (i) water spraying, (ii) roll compression, and (iii) salt-treatment and washing, were conducted according to previous report[12].

Measurements: The optical transmittance profiles of the AgNW films were characterized using a UV-visible spectrophotometer (Agilent 8453), and the sheet resistances were measured according to the four-point probe technique using Keithley 2182A and 6221 units. The surface morphologies of the samples were

measured using a tapping-mode AFM (D3100 Nanoscope V, Veeco). The chemical states of the samples were analyzed using X-ray photoemission spectroscopy (XPS, K-alpha, Thermo Fisher). For the tape test, a 5 mm wide and 20 mm long piece of 3M scotch tape was attached fully on the AgNWs film and then detached with a velocity of 1 cm/s. The water vapor transmission rate (WVTR) tests were performed to test the barrier properties of the samples by measuring the conductance of a Ca layer over time at 25°C and under 60% relative humidity (RH). WVTR value was calculated by the following equation[30],

$$\text{WVTR}[g/m^2 day] = -n\delta_{Ca}\rho_{Ca}\frac{d(G)}{d(t)}\frac{l}{w}\frac{M_{H_2O}}{M_{Ca}}\frac{Area(Ca)}{Area(Sample)}$$

in which n is molar equivalent of the degradation reaction ($n = 2$), δ_{Ca} and ρ_{Ca} is the resistivity (3.4×10^{-6} $\Omega \cdot m$) and density (1.55 g/cm^3) of Ca, respectively. $d(G)/d(t)$ is linear fitting in the conductance change versus time. l/w is the ratio between length and width of the Ca cell on glass. M_{H2O} and M_{Ca} are the molar masses of water vapor and Ca, respectively. $Area(Ca)/Area(Sample)$ represents the ratio of effective testing window to the deposited sample area (1 in this study).

Results and discussion

A schematic diagram showing the flexible AgNW TCEs prepared with an rGO-NH$_3^+$ adhesion promoter is illustrated in **Figure 1a**. The PEN substrate was first treated with UV-ozone to activate the hydroxyl groups on the substrate surface. GO-NH$_3^+$ and rGO-NH$_3^+$ suspensions[31] (PH=10) were then spray-coated onto the hydroxyl-functionalized PEN. The protonated amine groups (-NH$_3^+$) of the adhesion promoters could interact electrostatically with the hydroxyl groups of the UV-treated PEN substrate. The surface coverage levels of both adhesion promoters were controlled by varying the spray-coating time (between 5 and 30 s). The rGO-NH$_3^+$ samples prepared with four different coverage levels were prepared as shown in **Figure 1b**, representing that the rGO-NH$_3^+$ sheets were well spray-coated on the substrate, with lateral size ranging from 60 nm to 2 μm. Height profiles of the four samples in **Figure S1** demonstrated that the thickness of the rGO-NH$_3^+$ flakes ranged from 1 to 5 nm, corresponding to the few layers of rGO-NH$_3^+$ flakes. For comparison, the commercial positively charged poly(allylamine hydrochloride) (PAH)[32, 33] was used as an alternative adhesion promoter. The AgNW solution was coated onto the substrate using the Meyer rod coating method. The sheet resistance of the as-coated AgNW films was decreased by applying three post-treatment steps: (i) water spraying, (ii) roll compression, and (iii) salt treatment and washing, as described previously[12]. AgNWs are negatively charged[29] due to the presence of the oxo- and hydroxo- groups on the NW surfaces as a result of silver oxidation. The AgNWs could, therefore, be anchored to the positively charged rGO-NH$_3^+$ (GO-NH$_3^+$ or PAH) through strong electrostatic interactions. The insets of **Figure 1c** and **Figure S2** show optical images and scanning electron microscopy (SEM) images of the films prepared from pristine AgNWs or AgNWs in combination with the adhesion promoters PAH, GO-NH$_3^+$, or rGO-NH$_3^+$. No appreciable differences were observed between the films prepared with or without the adhesion promoters.

The optical transmittances of these four samples are shown in **Figure 1c**. The pristine AgNWs film exhibited an optical transmittance at 550 nm of 94%. The insertion of adhesion promoters between the AgNWs and the PEN substrate decreased the optical transmittance to 92% for PAH, 90% for GO-NH$_3^+$, and 89% for rGO-NH$_3^+$. In addition, optical transmittance of the AgNWs film decreased slightly with increasing surface coverage of GO-NH$_3^+$ (or rGO-NH$_3^+$) as shown in **Figure S3**. The slightly lower optical transmittance of the AgNWs film prepared with rGO-NH$_3^+$ (the relative dark color in the inset of **Figure 1c**), compared with GO-NH$_3^+$, suggested a slightly higher optical absorption due to the partial restoration of the π-electron system within the carbon structure after reducing the GO-NH$_3^+$ film[34, 35]. Note that the sheet resistances of the four samples were found to be 18.2 $\Omega \cdot$sq^{-1}, regardless of the adhesion promoter.

The chemical and mechanical stabilities of the AgNWs films prepared in combination with adhesion promoters were investigated. The pristine AgNWs films were immersed in a sonication bath (Powersonic 405, 350 W, operated in the low power mode) filled with isopropyl alcohol (IPA). The changes in the sheet resistances were monitored every 10 s, as shown in **Figure 2a**. The sheet resistance of the pristine AgNW films (18.2 $\Omega \cdot$sq^{-1}) increased abruptly to 32.7 $\Omega \cdot$sq^{-1} after only 4 s, and further ultrasonication yielded complete detachment of the AgNWs from the PEN substrate. The insertion of the positively charged adhesion promoters, such as PAH, GO-NH$_3^+$, or rGO-NH$_3^+$, however, dramatically enhanced the durability of the films to harsh ultrasonication conditions. For example, after ultrasonication for 80 s, the sheet resistances of the AgNW films were found to be 22, 23, or 26 $\Omega \cdot$sq^{-1} for the films treated with PAH, GO-NH$_3^+$, or rGO-NH$_3^+$, respectively. The conductive properties of the film prepared with PAH were maintained over a 110 s ultrasonication period, and the sheet resistance increased to 27 $\Omega \cdot$sq^{-1}. Better durability of the AgNW film prepared with PAH could be explained as follows. The partial charges of the protonated amine groups of PAH were more positive than those of GO-NH$_3^+$ or rGO-NH$_3^+$. Secondly, PAH was expected to provide a higher areal density of the protonated amine groups because one protonated amine group was present per polymer repeaing unit (will be discussed below). The AgNW films were also immersed in a variety of solvents, including water, ethanol, acetone, or IPA, and ultrasonicated for 20 s, as shown in **Figure 2b**. The pristine AgNW film became non-conductive after immersion into these four solvents due to the detachment of the AgNWs from the PEN substrate (open black bar). The AgNW films prepared with adhesion promoters showed enhanced chemical stabilities. Specifically, the PAH yielded a slightly better AgNWs film stability in ethanol, IPA, and acetone (18.5 $\Omega \cdot$sq^{-1}) compared with the stability conveyed by the other adhesion promoters, consistent with the results shown in **Figure 2a**. Unfortunately, the AgNWs were found to detach fully from the PEN substrate in water (open red bar) because the PAH polycations were soluble in water. By contrast, the AgNWs prepared with GO-NH$_3^+$ and rGO-NH$_3^+$ were stable under ultrasonication in water. PAH may not, therefore, be suitable as an adhesive in AgNW TCE-based waterproof electronic devices. The slightly higher sheet resistance of the AgNW prepared with rGO-NH$_3^+$, as compared with the sheet resistance of the AgNWs-GO-NH$_3^+$, was attributed to the partial

neutralization of the protonated amine groups in rGO-NH_3^+ through the formation of coordination bonds between the dangling nitrogen groups in the hydrazine moieties (–NNH_2) during the reduction of GO-NH_3^+[36, 37]. The ultrasonication test conducted in IPA was performed on the AgNW films deposited onto GO-NH_3^+ and rGO-NH_3^+ layers prepared with different surface coverage levels, as shown in **Figure S4**. A higher durability and a lower sheet resistance increase were observed with increasing surface coverage. These trends were attributed to the increased contact between the AgNWs and the GO-NH_3^+ (or rGO-NH_3^+) layer. The 3M scotch tape detachment tests were also performed to the AgNW films prepared with PAH and rGO-NH_3^+ (**Figure S5**). For the pristine AgNWs films, the AgNWs in the tape contact region were fully detached after one time detachment from the PEN substrate as shown in the inset of **Figure S5**. However, no obvious change in the sheet resistance was observed for both samples with adhesion promoters below 10 times detachment. The AgNWs with PAH exhibited slightly better stability than that of the AgNWs with rGO-NH_3^+, which is consistent with above ultrasonication test.

The mechanical stabilities of the AgNW films were investigated by measuring the sheet resistance under a compression or tension strain of ~ 0.3% (**Figure 2c**). The strain along the substrate length direction (ε_y) was caculated from from $\varepsilon_y = h/2R$, where h is the thickness of the PEN substrate and R is the radius of curvature (**Figure S6**). The relative sheet resistance (R/R_0) variations are shown in **Figure 2d**. The relative sheet resistance increased to 1.1 in the pristine AgNWs under a 0.3% strain, regardless of the compression or tension. The insertion of adhesion promoters enhanced the mechanical stabilities of the AgNW film. Under the same strain level, the AgNWs with rGO-NH_3^+ showed a higher sheet resistance compared to that of the PAH-AgNW films because the adhesion forces between the AgNWs and PAH were stronger. **Figure 2e** shows the results obtained from the fatigue test, which demonstrated that the sheet resistances of the films prepared from pristine AgNWs or AgNW in combination with adhesion promoters (rGO-NH_3^+ or PAH) were similar below 500 bending cycles. Differences between the sheet resistances were much larger beyond 1000 bending cycles as a result of the strong adhesion between the AgNWs and the rGO-NH_3^+ (or PAH). In addition, the rGO-NH_3^+ may contribute the current distribution across the mesh-type AgNWs even though its conductivity was low (several $k\Omega \cdot sq^{-1}$), which was identified by measuring the sheet resistances of various adhesion promoters without AgNWs as shown in **Figure S7**. This issue is important for organic electronic devices requiring uniform areal current distribution such as organic light emitting diodes and organic solar cells.

The changes in the chemical states induced by the interactions between the positively charged adhesion promoters and the AgNWs were investigated by performing X-ray photoelectron spectroscopy (XPS) measurements. **Figures 3a** and **3b** show the N 1s spectra of the PAH and rGO-NH_3^+ layers, respectively, before and after AgNW deposition. The N 1s spectra collected from PAH exhibited one distinct peak located at 402.18 eV, which corresponded to the protonated amines (-NH_3^+) in PAH (**Figure 3a**). Notably, after the deposition of the AgNWs onto the PAH layer, the peak shifted to lower binding energies (401.76 eV),

indicating that the chemical environment around the N atoms in PAH had changed. **Figure 3b** shows the N 1s spectra of the rGO-NH$_3^+$ layer before and after the AgNW deposition. The N 1s spectra included three components at 398.20, 399.82, and 402.91 eV, which were assigned to the amines, amides, and protonated amines, respectively. Similarly, the N 1s peak corresponding to -NH$_3^+$ and centered at 402.91 eV also shifted downward to 402.57 eV. The downward shifts in the -NH$_3^+$ peak after AgNW deposition originated from charge transfer from the negatively charged hydroxo- and oxo-groups on the AgNWs to the positively charged protonated amine groups in rGO-NH$_3^+$ (or PAH), indicating the presence of ionic interactions between the AgNWs and either adhesive promoter. Notably, the downward shift in the PAH-AgNW bonding (0.42 eV) was larger than that measured in rGO-NH$_3^+$ (0.34 eV), indicating the presence of stronger ionic interactions between the AgNWs and PAH[28, 38] (consistent with the chemical/mechanical stability results shown in **Figure 2**) due to the higher partial positive charge on the protonated amine group in the PAH molecules. In addition, the N 1s peak area of the protonated amine groups in PAH was larger than that in rGO-NH$_3^+$, which is originated from a higher areal density of the protonated amine groups for PAH compared with rGO-NH$_3^+$, thereby leading to better adhesion properties for PAH[39]. **Figure 3c** shows the Ag 3d XPS spectra obtained from the pristine AgNWs and the AgNW films prepared with PAH or rGO-NH$_3^+$. The peaks corresponding to the pristine AgNWs at 367.55 eV and 373.50 eV were assigned to Ag 3d$_{5/2}$ and 3d$_{3/2}$, respectively. In the AgNWs prepared with either PAH or rGO-NH$_3^+$, the peaks corresponding to Ag 3d$_{5/2}$ and 3d$_{3/2}$ were shifted toward lower binding energies by 0.23 and 0.30 eV, respectively. These results indicated that the chemical environment around the Ag atoms changed due to the ionic interactions between the AgNWs and rGO-NH$_3^+$ (or PAH).

Finally, the water vapor transmission rates (WVTRs) through the pristine AgNWs or the AgNW films prepared in combination with PAH, GO-NH$_3^+$, or rGO-NH$_3^+$ were measured as an indication of the water vapor permeability. WVTR is an important parameter for waterproof electronic device applications, which is measured to investigate the barrier performance of the encapsulation layers using the calcium (Ca) corrosion test method. This method monitors the Ca degradation by measuring a resistive change in the Ohmic behavior because Ca reacts easily with water vapor. A 200 nm thick calcium layer with an area of 1×1 cm^2 was thermally deposited between 100 nm thick patterned aluminum electrodes. A schematic diagram of the measurement set-up is shown in the inset of **Figure 4**. **Figure 4** shows the variations in the normalized conductance as a function of time at 25°C and a 60% relative humidity (RH). The WVTRs of the pristine AgNWs or the AgNW films prepared with PAH were 6.11 or 5.78, respectively. By contrast, both GO-NH$_3^+$ and rGO-NH$_3^+$ yielded enhanced water protection due to the closely packed hexagonal atomic structure. It is worthwhile noting that water vapor permeated relatively easily through GO (compared with rGO)[40] because the removal of the oxygen-containing groups blocked any permeation paths and enhanced the water barrier properties. The WVTR of the rGO-NH$_3^+$ (4.37) was slightly lower than that of GO-NH$_3^+$ (4.65).

Conclusions

In conclusion, ultrathin adhesion promoters that relied on positively charged GO or rGO (GO-NH$_3^+$ and rGO-NH$_3^+$) were prepared and tested for their utility in preparing highly stable AgNW TCEs. The insertion of ultrathin adhesion promoters between the AgNWs and the polymeric substrate dramatically enhanced the chemical and mechanical stabilities of the AgNW films due, presumably, to the ionic interaction between the negatively charged hydroxo- and oxo-groups on the AgNWs and the positively charged protonated amine groups in the rGO-NH$_3^+$ (or GO-NH$_3^+$). The closely packed hexagonal atomic structure of the ultrathin rGO-NH$_3^+$ adhesion promoter reduced the water permeability of the AgNW films, which is an important performance parameter for waterproof electronic device applications of AgNW TCEs. This work may play an important role in preparing high-quality TCEs for use in flexible and transparent electronics.

Nanoscale Accepted Manuscript

References

1   A. R. Madaria, A. Kumar, C. Zhou, *Nanotechnology*, 2011, **22**, 245201.

2   X. Wang, L. Zhi and K. Mullen, *Nano. lett.*, 2008, **8**, 323.

3   J. Wu, M. Agrawal, H. A. Becerril, Z. Bao, Z. Liu, Y. Chen, P. Peumans, *ACS Nano*, 2010, **4**, 43.

4   B. G. Lewis, D. C. Paine, *MRS bulletin*, 2000, **25**, 22.

5   Y. Leterrier, L. Médico, F. Demarco, J. A. E. Månson, U. Betz, M. F. Escolà, M. Kharrazi Olsson, F. Atamny, *Thin Solid Films*, 2004, **460**, 156.

6   S. De, P. E. Lyons, S. Sorel, E. M. Doherty, P. J. King, W. J. Blau, P. N. Nirmalraj, J. J. Boland, V. Scardaci, J. Joimel, J. N. Coleman, *ACS Nano*, 2008, **3**, 714.

7   F. Mirri, A. W. K. Ma, T. T. Hsu, N. Behabtu, S. L. Eichmann, C. C. Young, D. E. Tsentalovich, M. Pasquali, *ACS Nano*, 2012, **6**, 9737.

8   J. K. Wassei, R. B. Kaner, *Mater. Today.*, 2010, **13**, 52.

9   J. H. Park, D. Y. Lee, Y. H. Kim, J. K. Kim, J. H. Lee, J. H. Park, T. W. Lee, J. H. Cho, *ACS Appl. Mater. Inter.*, 2014, **6**, 12380.

10   S. Hong, J. Yeo, G. Kim, D. Kim, H. Lee, J. Kwon, H. Lee, P. Lee, S. H. Ko, *ACS Nano*, 2013, **7**, 5024.

11   J. Lee, P. Lee, H. Lee, D. Lee, S. S. Lee, S. H. Ko, *Nanoscale*, 2012, **4**, 6408.

12   S. J. Lee, Y.-H. Kim, J. K. Kim, H. Baik, J. H. Park, J. Lee, J. Nam, J. H. Park, T.-W. Lee, G.-R. Yi, J. H. Cho, *Nanoscale*, 2014, **6**, 11828.

13   Y. M. Chang, W. Y. Yeh, P. C. Chen, *Nanotechnology*, 2014, **25**, 285601.

14   S. Ye, A. R. Rathmell, Z. Chen, I. E. Stewart, B. J. Wiley, *Adv. Mater.*, 2014, **26**, 6670.

15   S. Nam, M. Song, D. H. Kim, B. Cho, H. M. Lee, J. D. Kwon, S. G. Park, K. S. Nam, Y. Jeong, S. H. Kwon, Y. C. Park, S. H. Jin, J. W. Kang, S. Jo, C. S. Kim, *Sci. Rep.*, 2014, **4**, 4788.

16   P. Lee, J. Lee, H. Lee, J. Yeo, S. Hong, K. H. Nam, D. Lee, S. S. Lee, S. H. Ko, *Adv. Mater.*, 2012, **24**, 3326.

17   D. S. Leem, A. Edwards, M. Faist, J. Nelson, D. D. Bradley, J. C. de Mello, *Adv. Mater.*, 2011, **23**, 4371.

18   R. Zhu, C.-H. Chung, K. C. Cha, W. Yang, Y. B. Zheng, H. Zhou, T.-B. Song, C.-C. Chen, P. S. Weiss, G. Li, Y. Yang, *ACS Nano*, 2011, **5**, 9877.

19   J. Lee, P. Lee, H. B. Lee, S. Hong, I. Lee, J. Yeo, S. S. Lee, T.-S. Kim, D. Lee, S. H. Ko, *Adv. Func. Mater.*, 2013, **23**, 4171.

20   L. Yang, T. Zhang, H. Zhou, S. C. Price, B. J. Wiley, W. You, *ACS Appl. Mater. Inter.*, 2011, **3**, 4075.

21   D. Y. Choi, H. W. Kang, H. J. Sung, S. S. Kim, *Nanoscale*, 2013, **5**, 977.

22   A. Kim, Y. Won, K. Woo, C.-H. Kim, J. Moon, *ACS Nano*, 2013, **7**, 1084.

23   D. S. Ghosh, T. L. Chen, V. Mkhitaryan, N. Formica, V. Pruneri, *Appl. Phys. Lett.*, 2013, **102**, 221111.

Nanoscale Accepted Manuscript

24   I. K. Moon, J. I. Kim, H. Lee, K. Hur, W. C. Kim, H. Lee, *Sci. Rep.*, 2013, **3**, 1112.

25   X. Zhang, X. Yan, J. Chen, J. Zhao, *Carbon*, 2014, **69**, 437.

26   J. Liang, L. Lu, K. Tong, Z. Ren, W. Hu, X. Niu, Y. Chen, Q. Pei, *ACS Nano*, 2014, **8**, 1590.

27   Y. Li, P. Cui, L. Wang, H. Lee, K. Lee, H. Lee, *ACS Appl. Mater. Inter.*, 2013, **5**, 9155.

28   H. Lee, K. Lee, J. T. Park, W. C. Kim, H. Lee, *Adv. Func. Mater.*, 2014, **24**, 3276.

29   Q. N. Luu, J. M. Doorn, M. T. Berry, C. Jiang, C. Lin, P. S. May, *J. Colloid Interface Sci.*, 2011, **356**, 151.

30   W. Xiao, D. Yu, S. F. Bo, Y. Y. Qiang, Y. Dan, C. Ping, D. Y. Hui, Z. Yi, *RSC Adv.*, 2014, **4**, 43850

31   D. W. Lee, T.-K. Hong, D. Kang, J. Lee, M. Heo, J. Y. Kim, B.-S. Kim, H. S. Shin, *J. Mater. Chem.*, 2011, **21**, 3438.

32   S. W. Cranford, C. Ortiz, M. J. Buehler, *Soft Matter.*, 2010, **6**, 4175.

33   M. R. Kreke, A. S. Badami, J. B. Brady, R. M. Akers, A. S. Goldstein, *Biomaterials*, 2005, **26**, 2975.

34   S. Pei, H.-M. Cheng, *Carbon*, 2012, **50**, 3210.

35   G. Williams, B. Seger, P. V. Kamat, *ACS Nano*, 2008, **2**, 1487.

36   S. Mao, H. Pu, J. Chen, *RSC Adv.*, 2012, **2**, 2643.

37   S. Stankovich, D. A. Dikin, R. D. Piner, K. A. Kohlhaas, A. Kleinhammes, Y. Jia, Y. Wu, S. T. Nguyen, R. S. Ruoff, *Carbon*, 2007, **45**, 1558.

38   J. Cazes, *Analytical Instrumentation Handbook*, CRC Press, England, 2004.

39   S. M. Lee, *Handbook of composite reinforcements*. VCH Publishers, Inc. Germany, 1993.

40   R. R. Nair, H. A. Wu, P. N. Jayaram, I. V. Grigorieva, A. K. Geim, *Science*, 2012, **335**, 442.
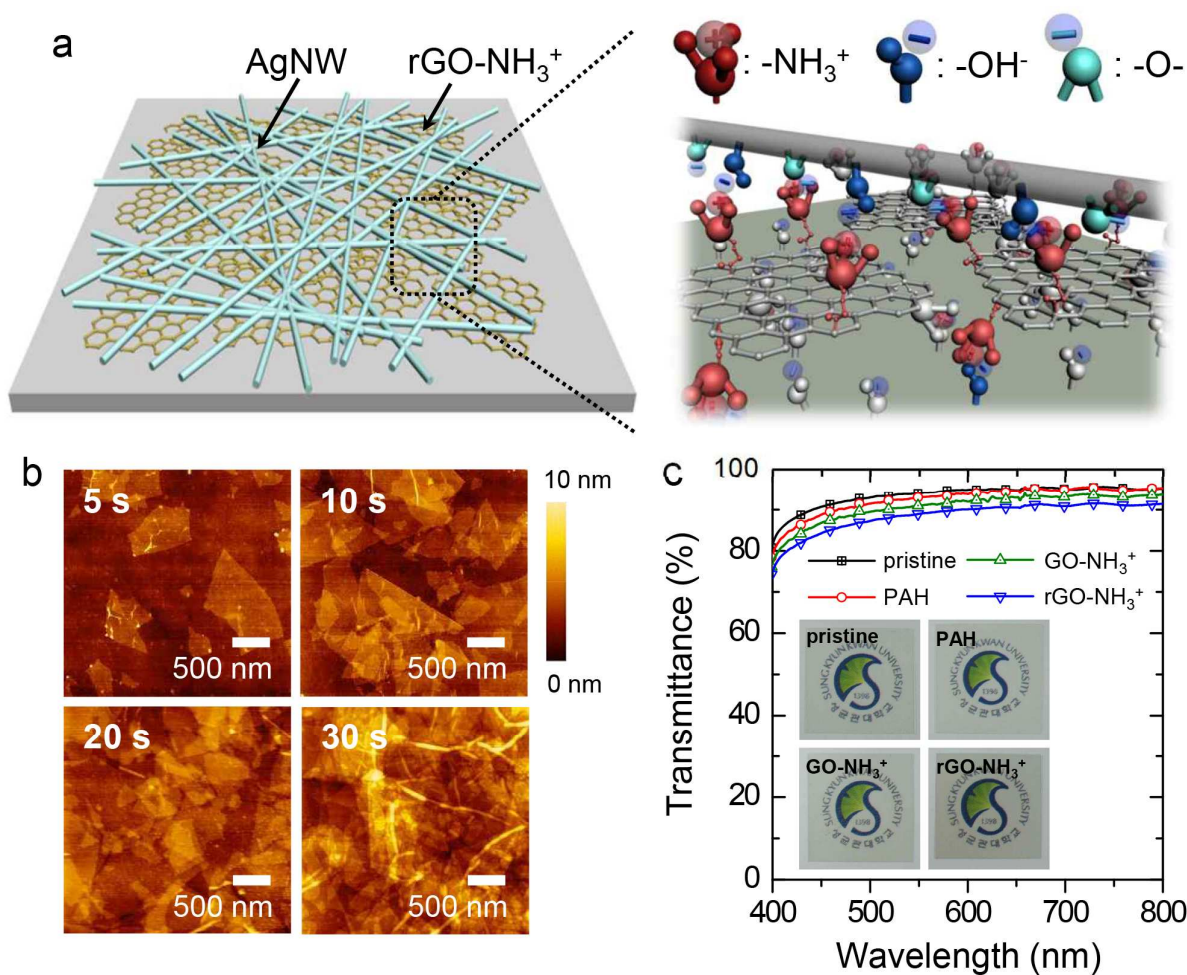
Figure 1. (a) Schematic illustration of the flexible AgNW TCEs prepared with the rGO-NH$_3^+$ adhesion promoter. (b) Atomic force microscopy (AFM) images of the rGO-NH$_3^+$ layers prepared with four different coverage levels. (c) The optical transmittances of the films prepared from pristine AgNW or AgNW in combination with the adhesion promoters PAH, GO-NH$_3^+$, or rGO-NH$_3^+$. The time period over which the GO-NH$_3^+$, or rGO-NH$_3^+$ suspensions were spray-coated was 20 s. The inset shows photographic images of the films.
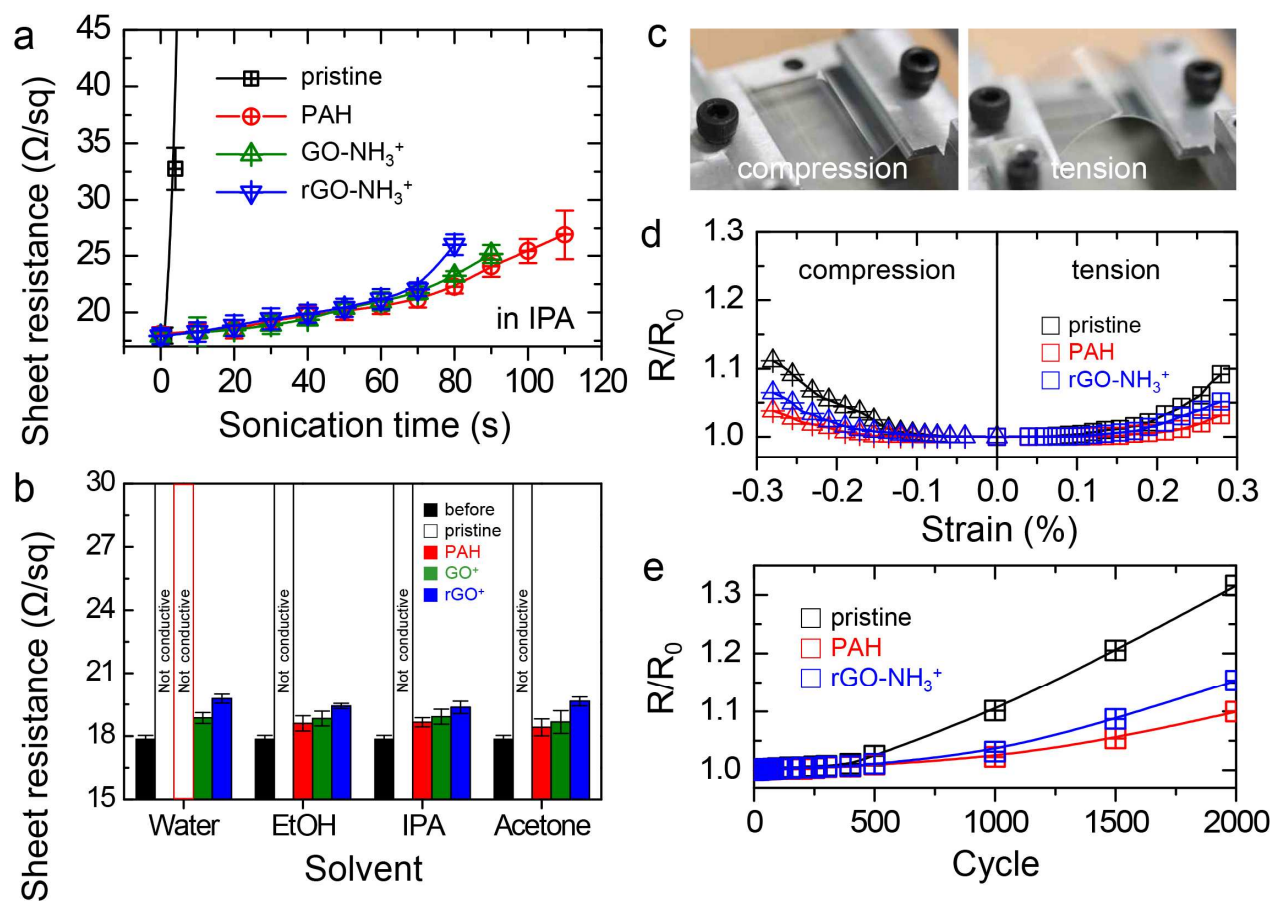
Figure 2. (a) Sheet resistance as a function of the time period over which the films prepared from pristine AgNWs or AgNWs in combination with the adhesion promoters PAH, GO-NH$_3^+$, and rGO-NH$_3^+$ were ultrasonicated in IPA. (b) The sheet resistances of the four AgNW films after ultrasonication in various solvents, including water, ethanol, acetone, or IPA for 20 s. (c) Experimental setup used in the bending test. (d) R/R$_0$ as a function of the strain level (0 ~ 0.3%). (e) R/R$_0$ as a function of the cycle number under a 0.1% strain tension.
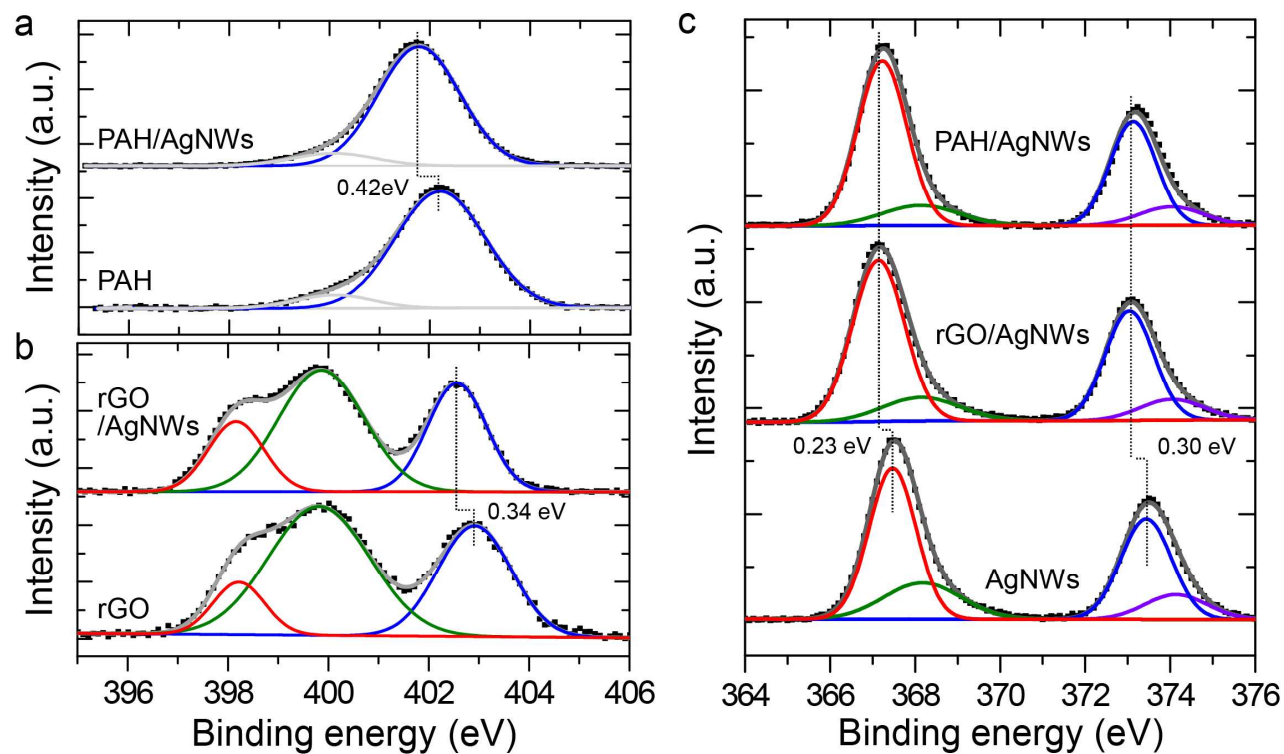
Figure 3. (a) High-resolution XPS N 1s spectra obtained from a PAH layer before and after AgNW deposition. The weak gray peak originated from the plastic substrate. (b) High-resolution XPS N 1s spectra of the rGO-NH$_3^+$ layers before or after AgNW deposition. (c) High-resolution Ag 3d XPS spectra obtained from the pristine AgNWs or Ag NWs prepared in combination with PAH or rGO-NH$_3^+$.
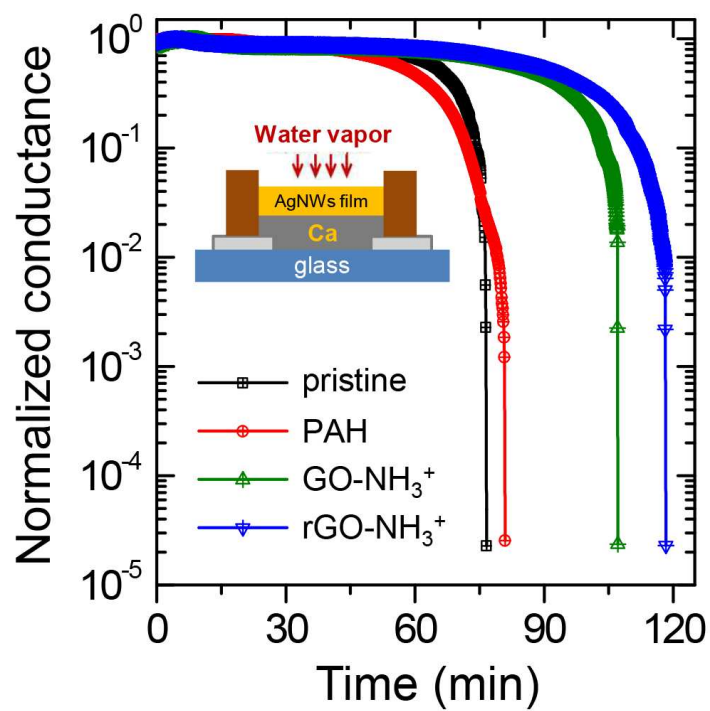
Figure 4. WVTR test results obtained from the films prepared from the pristine AgNWs or the AgNWs in combination with the adhesion promoters PAH, $GO\text{-}NH_3^+$, or $rGO\text{-}NH_3^+$.

TOC Figure
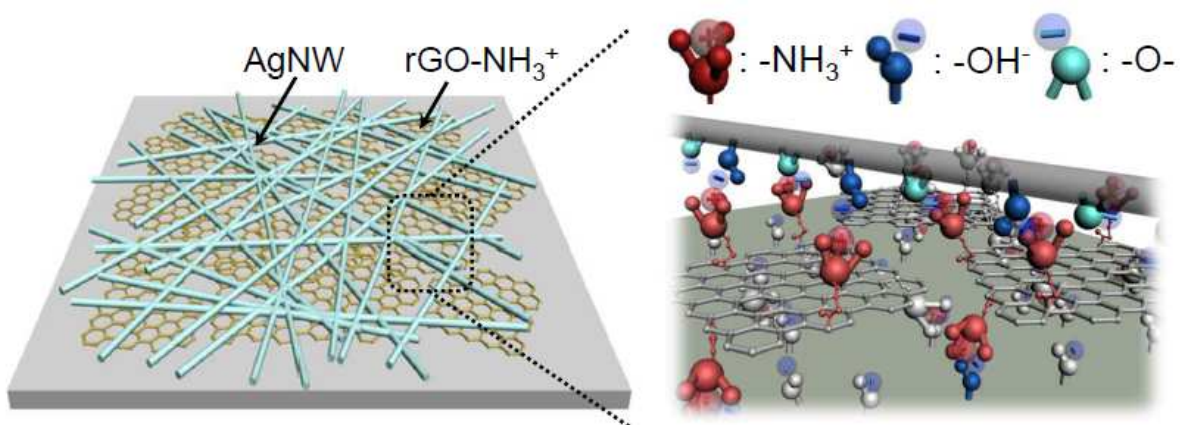
Ultrathin conductive adhesion promoter using positively charged reduced graphene oxide (rGO-NH$_3^+$) are demonstrated for preparing highly stable AgNW transparent electrodes.